A Global 3-D Model Evaluation of the Atmospheric Budgets of HCN and CH_3CN: Constraints From Aircraft Measurements Over the Western Pacific

Qinbin Li, Daniel J. Jacob, Robert M. Yantosca, Colette L. Heald
Department of Earth and Planetary Sciences and Division of Engineering and Applied Sciences, Harvard University, Cambridge, MA

Hanwant B. Singh
NASA Ames Research Center, Moffett Field, CA

Makoto Koike
Department of Earth and Planetary Science, University of Tokyo, Tokyo, Japan

Yongjing Zhao
Department of Physics, University of Toronto, Toronto, Canada.

Glen W. Sachse
NASA Langely Research Center, Hampton, VA

David G. Streets
Argonne National Laboratory, Argonne, IL

Short title: ATMOSPHERIC BUDGETS OF HCN AND CH_3CN

Abstract.

We construct global atmospheric budgets of HCN and CH_3CN through a 3-D simulation of the HCN-CH_3CN-CO system constrained and evaluated with aircraft observations from the TRACE-P mission over the NW Pacific in February-April 2001. Observed background vertical gradients of HCN and CH_3CN imply a dominant ocean sink for both gases, with deposition velocity of 0.13 $cm\,s^{-1}$ for both and saturation ratios of 0.79 for HCN and 0.88 for CH_3CN. Observations for both gases in the free troposphere implied a dominant source from biomass burning. Enhancement of HCN observed in Chinese urban plumes is attributed tentatively to residential coal burning. Biomass burning and residential coal burning emission ratios relative to CO of 0.27% and 1.6% respectively for HCN, and of 0.20% and 0.25% respectively for CH_3CN, are consistent with observations in biomass burning and Chinese urban plumes, and provide the best fit in the model for simulation of observed TRACE-P vertical profiles, HCN-CH_3CN-CO correlations, as well as long-term records of HCN columns and CH_3CN observations over the northern Indian Ocean. Biomass burning and residential coal burning contribute 0.63 and 0.2 $Tg\,N\,yr^{-1}$ respectively to global HCN and 0.47 and 0.03 $Tg\,N\,yr^{-1}$ respectively to CH_3CN. Ocean uptake is the dominant sink for both gases, with oxidation by OH representing an additional minor sink. The resulting tropospheric lifetimes are 5.3 months for HCN and 5.8 months for CH_3CN. The model predicts very low HCN and CH_3CN concentrations at high southern latitudes, reflecting the assumption of uniform saturation ratio; observations in that region are needed. In the free troposphere, the dominance of biomass burning sources (70-85% for HCN and 90-95% for CH_3CN) implies that both gases can be used as biomass burning tracers. More work is needed to identify the urban source apparent in the Chinese plume observations.

1. Introduction

Hydrogen cyanide (HCN) and methyl cyanide (CH_3CN, also called acetonitrile) are atmospheric tracers of biomass burning [*Lobert et al.*, 1990; *Holzinger et al.*, 1999] and could play a non-negligible role in the nitrogen cycle [*Li et al.*, 2000]. Ocean uptake has been hypothesized as their dominant sink, with corresponding lifetimes of a few months [*Hamm and Warneck*, 1990; *Li et al.*, 2000]. However, their atmospheric budgets are still poorly understood. We use here a global 3-D model analysis of HCN and CH_3CN observations in Asian outflow from the TRACE-P aircraft mission over the NW Pacific [*Singh et al.*, this issue] to improve the constraints on the sources and sinks of these two gases. The TRACE-P data represent the first in situ measurements for HCN in the troposphere, and one of the first for CH_3CN. Previous data for HCN are from remote sensing of the total column at several sites around the world [*Mahieu et al.*, 1995, 1997; *Rinsland et al.*, 1999, 2000, 2001, 2002; *Zhao et al.*, 2000, 2002]. Previous in situ measurements of CH_3CN have been made over the Indian Ocean [*de Laat et al.*, 2001] and over the Amazon [*Williams et al*, 2001].

It is well established from laboratory and field experiments that biomass burning is a major source for both HCN (0.1-3.2 $\mathrm{Tg\,N\,yr^{-1}}$) and CH_3CN (0.2-1.1 $\mathrm{Tg\,N\,yr^{-1}}$) (Table 1). It is also well established that sources from automobile exhaust and industrial processes are negligible in comparison [*Lobert et al.*, 1991; *Bange*, 2000; *Holzinger et al.*, 2001]. A recent field experiment indicates no emission of HCN from domestic biofuels [*Bertschi et al.*, 2002]. Atmospheric sinks of HCN and CH_3CN from reaction with OH and $O(^1D)$, photolysis, and scavenging by precipitation yield lifetimes of a few years [*Cicerone and Zellner*, 1983; *Brasseur et al.*, 1983]. The solubilities of HCN and CH_3CN are sufficiently high for ocean uptake to impose atmospheric lifetimes of a few months if loss in the oceanic mixed layer is sufficiently rapid [*Hamm and Warneck*, 1990; *Li et al.*, 2000]. There is some evidence that HCN and CH_3CN are consumed biologically in the ocean [*Singh et al.*, this issue]. *Li et al.* [2000] showed in a global 3-D model study that the observed seasonal variation of the HCN column in different regions of the world is consistent with a scenario where biomass burning provides the main source and ocean uptake provides the main sink. They inferred a global HCN biomass burning source of 1.4-2.9 $\mathrm{Tg\,N\,yr^{-1}}$, and an oceanic saturation ratio of 0.83 or less. Observed vertical gradients of HCN and CH_3CN in remote marine air in TRACE-P confirm the importance of the ocean sink [*Singh et al.*, this issue].

The TRACE-P mission was conducted in February-April 2001 over the NW Pacific to study the transport and chemical evolution of Asian outflow over the Pacific [*Jacob et al.*, this

issue]. It used two NASA aircraft, a DC-8 and a P-3B, operating out of Hong Kong and Japan, and with additional transit flights and sorties over the North Pacific. Biomass burning in SE Asia is an important component of Asian outflow in spring [*Liu et al.*, 1999; *Chan et al.*, 2000; *Bey et al.*, 2001b]. During TRACE-P, Asian biomass burning and anthropogenic sources had contributions of similar magnitude to CO concentrations observed in Asian outflow [*Liu et al.*, this issue; *Heald et al.*, this issue].

Both HCN and CH_3CN were measured by gas chromatography aboard the DC-8 aircraft [*Singh et al.*, this issue]. The measurement accuracy was about $\pm$25% and the detection limit 30 pptv. Other measurements aboard the DC-8 included CO, perchloroethylene (C_2Cl_4), and methyl chloride (CH_3Cl). CO is a tracer of combustion. C_2Cl_4, a synthetic organic chemical used in dry cleaning, is an anthropogenic pollution tracer. CH_3Cl can be used as a biomass burning tracer in Asian outflow [*Blake et al.*, 2001]. These complementing measurements can be used to place constraints on the sources of HCN and CH_3CN [*Singh et al.*, this issue]. Some of the results shown in *Singh et al.* [this issue] are reproduced here for purpose of comparison to model results. Throughout this paper, model comparisons to observations will use model results sampled along the DC-8 flight paths. All linear regressions shown in this paper are calculated using the reduced major axis (RMA) method, which allows for errors in both variables.

2. Model Simulation

We simulate the distributions of HCN, CH_3CN, and CO observed in TRACE-P with the GEOS-CHEM global 3-D model of tropospheric chemistry. A detailed description of the model is presented by *Bey et al.* [2001a]. We use here GEOS-CHEM version 4.33 (see http://www-as.harvard.edu/chemistry/trop/geos). The model is driven by assimilated meteorological fields from the Goddard Earth Observing System (GEOS) of the NASA Data Assimilation Office (DAO). We use meteorological fields for 2000-2001 (GEOS-3) which are provided with 6-hour temporal resolution (3-hour for surface variables and mixed layer depths), $1^\circ \times 1^\circ$ horizontal resolution, and 48 vertical sigma levels. We degrade the horizontal resolution to $2^\circ \times 2.5^\circ$ for application in GEOS-CHEM. The simulations are conducted for a 16-month period (January 2000-April 2001). The first 13 months are used for initialization and we present results for the February-April 2001 TRACE-P period.

Sources and sinks of HCN and CH_3CN in the model are described in section 3. The

CO simulation follows that of *Duncan et al.* [2002] and uses archived OH concentration fields (monthly mean) from a full-chemistry simulation [*Li et al.*, 2002] to calculate CO loss. Anthropogenic emissions are as described in *Duncan et al.* [2002] except for Asia, where the *Streets et al.* [this issue] inventory is used. Biomass burning emissions are as described in *Heald et al.* [this issue]. The total biomass burning CO source is 487 $\mathrm{Tg\,CO\,yr^{-1}}$ for 2000, while the total CO sources from fossil fuel and biofuel are 497 and 200 $\mathrm{Tg\,CO\,yr^{-1}}$, respectively. For the TRACE-P period (February-April 2001), the global biomass burning CO source is 129 Tg CO and about half of that source is in SE Asia.

Since the model simulations of HCN, CH_3CN, and CO as implemented here are linear with respect to their sources, we resolve the contributions from different source regions and source types in the model by using tagged tracers [*Bey et al.*, 2001b], which can then be added to reconstitute the full concentration field. Tagged tracers resolve sources from biomass burning, biofuels, and residential coal burning, for Asia and for the rest of the world.

3. Model Sources and Sinks of HCN and CH_3CN

3.1. Sinks

3.1.1. Ocean Uptake Constraints on ocean uptake for HCN and CH_3CN can be obtained from the vertical gradients of concentrations measured in background air over the North Pacific during TRACE-P [*Singh et al.*, this issue]. We implement this constraint here by using the observed gradients to infer a saturation ratio for these two gases that we can then extrapolate globally in the 3-D model simulation.

Figure 1 shows the vertical distributions of HCN, CH_3CN, and CO observed for the ensemble of the data in TRACE-P (dots and red lines). The CO mixing ratios decrease from the boundary layer to the free troposphere, while the opposite is seen in the mixing ratios of HCN and CH_3CN. This is consistent with an ocean sink for HCN and CH_3CN but could also reflect the dominant biomass burning source for these two gases, in contrast to the large fossil fuel source for CO. Biomass burning outflow during TRACE-P was largely confined to the free troposphere, while there was considerable fossil fuel outflow in the boundary layer [*Carmichael et al.*, this issue; *Liu et al.*, this issue].

Figure 2 shows the vertical distributions of HCN and CH_3CN (dots and red lines) observed in TRACE-P over the North Pacific under background conditions, defined here as CO $<$ 120 ppbv and C_2Cl_4 $<$ 10 pptv [*Singh et al.*, this issue]. Both gases show significantly

reduced mixing ratios in the marine boundary layer compared with their free tropospheric values. Asian outflow influence for these conditions is minimal, and the shape of the profiles is evidence for ocean uptake. Median mixing ratios at 2-4 km are 201 pptv for HCN and 134 pptv for CH_3CN, while the corresponding values at 0-2 km are 161 pptv and 106 pptv, respectively.

Following *Singh et al.* [this issue], the deposition velocities of HCN and CH_3CN to the ocean can be derived using a box model of the marine boundary layer (MBL) with no divergence of horizontal flux [*Lenschow*, 1983]. We calculate the flux across the MBL top as the concentration difference between 2-4 km (C_{FT}) and 0-2 km (C_{MBL}) multiplied by an entrainment velocity K_e = 0.5 $\mathrm{cm\,s^{-1}}$ [*Heikes et al.*, 1996]. At steady state, this flux must be balanced by the ocean uptake flux ($v_d C_{MBL}$, where v_d is the deposition velocity). Loss by reaction with OH is negligible, since both HCN and CH_3CN can be considered chemically inert on the time scale for MBL turnover (a few days). It follows that

$$v_d = K_e \left(\frac{C_{FT}}{C_{MBL}} - 1 \right) \tag{1}$$

The resulting deposition velocity is 0.13 $\mathrm{cm\,s^{-1}}$ for both HCN and CH_3CN.

The comparable deposition velocities despite greater solubility of CH_3CN imply faster consumption of HCN/CN^- in the oceans (see discussion below). *de Laat et al.* [2001] previously inferred a deposition velocity of 0.01-0.05 $\mathrm{cm\,s^{-1}}$ for CH_3CN to the ocean in order to explain CH_3CN mixing ratios observed in South Asian outflow to the Indian Ocean (INDOEX mission). *Warneke and de Gouw* [2001] estimated a deposition velocity of 0.34 $\mathrm{cm\,s^{-1}}$ for CH_3CN from ship measurements taken during an oceanic upwelling event. They attributed the higher value compared to *de Laat et al.* [2001] to the lower surface temperature and higher biological activity in the upwelling water. More recently, *de Gouw et al.* [2002] estimated a deposition velocity of 0.17 $\mathrm{cm\,s^{-1}}$ for CH_3CN from aircraft measurements over the NE Pacific.

Using a two-layer film model for air-to-sea exchange [*Liss and Slater*, 1974], *Singh et al.* [this issue] estimated saturation ratios of 0.77 for HCN and 0.83 for CH_3CN from their TRACE-P data. Saturation ratio is related to deposition velocity by

$$v_d = (1 - S) K_g \tag{2}$$

where K_g is the air-to-sea transfer velocity and is calculated from conductances for mass transfer in the gas and liquid phases, for which we adopt the *Asher* [1997] and the *Nightingale*

et al. [2000] parameterizations, respectively. The resulting saturation ratios are 0.79 for HCN and 0.88 for CH_3CN. The difference with *Singh et al.* [this issue] reflects different assumptions on the parameterizations of conductances for mass transfer. In our 3-D model calculation we extrapolate these saturation ratios globally, resulting in atmospheric lifetimes against ocean uptake of six months for HCN and 8 months for CH_3CN.

At steady state, the ocean uptake flux must be balanced by consumption in the oceanic mixed layer (OML)

$$v_d C_{MBL} = \frac{Z}{\tau} C_{OML} \tag{3}$$

$$S = H \frac{C_{OML}}{C_{MBL}} \tag{4}$$

$$\tau = \frac{Z}{H} \frac{S}{v_d} = \frac{Z}{H} \left(\frac{1}{v_d} - \frac{1}{K_g} \right) \tag{5}$$

where Z is the oceanic mixed layer depth (about 50 m for the middle-latitude North Pacific in March [*Kara et al.*, 2000]), τ is the lifetime against consumption in the OML, C_{OML} is the concentration in the OML, and H is the dimensionless Henry's law constant defined as the ratio of the concentration in air to that in seawater. Values for H at 298 K are 3.4×10^{-3} ($\Delta H_{298}/R$ = 5000 K) for HCN and 7.6×10^{-4} ($\Delta H_{298}/R$ = 4100 K) for CH_3CN [*Sander*, 1999]. The resulting lifetimes against consumption in the OML are three months for $HCN(aq)/CN^-$ and 14 months for $CH_3CN(aq)/CN^-$.

3.1.2. Other Sinks Additional known losses for atmospheric HCN and CH_3CN are reactions with OH and $O(^1D)$, photolysis, and precipitation scavenging. Of these, only reaction with OH is significant [*Cicerone and Zellner*, 1983; *Brasseur et al.*, 1983] and is implemented in the model using rate constants from *Wine* [2002] for HCN and *DeMore et al.* [1997] for CH_3CN, with monthly mean OH fields from a full chemistry simulation [*Li et al.*, 2002]. The recent laboratory study of *Wine* [2002] indicates a factor of three lower rate constant for the HCN-OH reaction (low-pressure limit 7.4×10^{-33} $cm^6\,molecule^{-2}\,s^{-1}$; high-pressure limit $9.0 \times 10^{-15}\,(T/300)^{3.2}$ $cm^3\,molecule^{-1}\,s^{-1}$, where T is temperature) than previously measured [*Fritz et al.*, 1984]. The corresponding lifetimes against oxidation by OH are 4.3 years for HCN and 2.2 years for CH_3CN, much longer than the lifetimes against ocean uptake.

3.2. Sources

3.2.1. Biomass Burning Both HCN and CH_3CN are mainly emitted in the low-temperature smoldering phase of biomass burning, similarly to CO [*Lobert et al.*, 1990].

Different fuel types and fire temperatures result in different emission ratios [*Lobert et al.*, 1991]. Past studies have indicated a large range of molar emission ratios for HCN (0.03-1.1%) and a narrower range for CH_3CN (0.12-0.25%) [*Lobert et al.*, 1991; *Hurst et al.*, 1994a, b; *Yokelson et al.*, 1997, 1999, 2002; *Holzinger et al.*, 1999; *Goode et al.*, 2000]. Emission ratios throughout this paper are in molar units relative to CO. When compounded with a range of global biomass burning CO emission estimates (200-800 $\mathrm{Tg\,CO\,yr^{-1}}$), one obtains global biomass burning sources of 0.1-3.2 $\mathrm{Tg\,N\,yr^{-1}}$ for HCN and 0.1-1.1 $\mathrm{Tg\,N\,yr^{-1}}$ for CH_3CN (Table 1).

The recent review of *Andreae and Merlet* [2001] recommends biomass burning HCN emission ratios of 0.05% (savanna and grassland) and 0.15% (tropical and extratropical forests) and a biomass burning CH_3CN emission ratio of 0.11% for all vegetation types. The HCN recommendation for savanna and grassland is based on field experiments in Australia [*Hurst et al.*, 1994a, b]. Recent measurements in African savanna fires show much higher HCN emission ratios ($0.85 \pm 0.29\%$) [*Yokelson et al.*, 2002]. By averaging measurements of biomass burning emissions from different fuel types and from different regions of the world, *Goode et al.* [2000] found an average biomass burning HCN emission ratio of 0.34%, much higher than the *Andreae and Merlet* [2001] value.

Correlations with CO in the TRACE-P observations provide important constraints on the emissions of HCN and CH_3CN. *Singh et al.* [this issue] used these correlations in biomass burning plumes to derive emission ratios of $0.27 \pm 0.12\%$ for HCN and $0.15 \pm 0.05\%$ for CH_3CN. The HCN emission ratio is consistent with the average value reported by *Goode et al.* [2000], and is also in accord with the value of 0.28% estimated by *Heald et al.* [this issue] based on multivariate analysis of the TRACE-P CO and HCN data. The CH_3CN emission ratio is consistent with the *Andreae and Merlet* [2001] value. We find in GEOS-CHEM that the best fit to the TRACE-P observations of HCN, CH_3CN, and CO, and to the global HCN column data is obtained with biomass burning emission ratios of 0.27% for HCN and 0.20% for CH_3CN, consistent with *Singh et al.* [this issue]; we use these values in the simulations presented here. The corresponding sources of HCN and CH_3CN are 0.63 and 0.47 $\mathrm{Tg\,N\,yr^{-1}}$, respectively (Table 2), within the range of past estimates (Table 1).

3.2.2. Chinese Urban Source It is well established that HCN and CH_3CN are produced in the early stages of high-temperature combustion but are subsequently oxidized within the combustion chamber [*Flagan and Seinfeld*, 1988]. Direct measurements in automobile exhaust [*Lobert et al.*, 1991; *Holzinger et al.*, 2001] as well as aircraft measurements by *Singh*

et al. [this issue] and *de Gouw et al.* [2002] over southern California confirm that this source is negligible compared to biomass burning (Table 1) and we do not include it in the present study.

However, TRACE-P observations showed a strong enhancement of HCN, and a much weaker enhancement of CH_3CN, in Chinese urban plumes sampled in the MBL less than two days downwind of the source [*Singh et al.,* this issue]. Figure 3 shows the HCN and CH_3CN correlations with CO observed in three major Chinese urban plumes (DC-8 flights 9, 12, 13) sampled in the MBL during TRACE-P. Asian outflow in the MBL was in general advected behind cold fronts and was devoid of biomass burning influence [*Carmichael et al.,* this issue; *Liu et al.,* this issue]. The peak mixing ratios of HCN and CO in the urban plumes are 1.5 ppbv and 1 ppmv, respectively, while the peak mixing ratio for CH_3CN is 300 pptv, much less enhanced. These peak mixing ratios were associated with high mixing ratios of CH_3Cl (see Figure 7a of *Singh et al.* [this issue]) and carbonyl sulfide (COS). The HCN-CO and CH_3CN-CO correlations show slopes of 0.17% and 0.04%, respectively (Figure 3).

Although there is widespread biofuel use in China [*Streets et al,* this issue], data from Africa indicate negligible nitrile emission from biofuels [*Bertschi et al.,* 2002; *Yokelson et al.,* 2002]. Also, the CH_3CN/HCN enhancement ratio is much lower in the Chinese urban plumes than in biomass burning plumes (Figure 4). *Singh et al.* [this issue] suggested that the enhancements of CH_3Cl and COS correlated with enhanced HCN in the Chinese urban plumes could indicate a source from hard coal burning, and we follow that suggestion here. Clearly, further work is needed identify the Chinese source of nitriles.

The *Streets et al.* [this issue] inventory includes explicitly residential coal burning source for Asia. For the rest of the world, this source is taken from the EDGAR 3.2 emission inventory [*Olivier and Berdowski,* 2001]. In *Duncan et al.* [2002], residential coal burning was lumped into fossil fuel source. We did not bother to separate it out because it is only a small fraction of the total anthropogenic source. The resulting CO source from residential coal burning is 30 $\mathrm{Tg\,CO\,yr^{-1}}$ in the model.

We estimate the residential coal burning emission ratios of HCN and CH_3CN from the three Chinese urban plumes observed in TRACE-P (Figure 3). According to the *Streets et al.* [this issue] emission inventory, emissions from residential coal burning account for 7% of the total CO emissions for China overall. Combined with the slopes of the HCN-CO and CH_3CN-CO correlations observed in the Chinese urban plumes (Figure 3), we obtain residential coal burning emission ratios of 2.4% for HCN and 0.6% for CH_3CN. Simulation

of the TRACE-P data with GEOS-CHEM (section 4) indicates a best fit for residential coal burning emission ratios of 1.6% for HCN and 0.25% for CH_3CN. Additionally, we find in the GEOS-CHEM that to achieve the best fit to the observed HCN-CH_3CN-CO correlations in the boundary layer, we have to double the residential coal burning source from Asia. This leads us to reduce the residential coal burning source from the rest of the world by a factor of eight to achieve a best fit to the observed vertical distributions of HCN and CH_3CN.

When scaling the above emission ratios by the fraction of urban CO from residential coal burning in China, the resulting HCN/CO source ratio (0.24% for Shanghai, for example) is comparable to biomass burning (0.27%) while the resulting CH_3CN/CO source ratio (0.04% for Shanghai, for example) is much lower than biomass burning (0.20%). The corresponding global sources are 0.2 for HCN and 0.03 $\mathrm{Tg\,N\,yr^{-1}}$ for CH_3CN (Table 2). This source could have a seasonal variation associated with heating [*Streets et al.*, this issue], but uncertainties are sufficiently large that we do not bother to include it here.

3.2.3. Biogenic Source There is indication that HCN is produced by higher plants [see *Cicerone and Zellner*, 1983, and references therein]. Recent laboratory results by *Fall et al.* [2001] show that wounded clover releases HCN in addition to large amounts of acetone. In the TRACE-P data, HCN is correlated with both acetone (r = 0.81, slope = 0.33 $\mathrm{pptv\,ppbv^{-1}}$, n = 746) and methanol (r = 0.86, slope = 136.6 $\mathrm{pptv\,ppbv^{-1}}$, n = 744), which have strong biogenic sources. In particular, methanol is generally considered a tracer for continental biogenic emissions [*Heikes et al.*, 2002]. Figure 5 (top panel) shows the correlation of HCN with methanol observed during TRACE-P. A similarly strong correlation was found for CH_3CN. The biogenic source of methanol is estimated to be 50-280 $\mathrm{Tg\,yr^{-1}}$ [*Heikes et al.*, 2002]. If the HCN-methanol correlation were to reflect a biogenic source, then the implied biogenic HCN source would be 3-17 $\mathrm{Tg\,N\,yr^{-1}}$, far too large to be reconciled with the observed HCN concentrations [*Li et al.*, 2000]. Additionally, the highest methanol and HCN concentrations in TRACE-P were observed in the Chinese urban plumes. Methanol in TRACE-P was also strongly correlated with CO (r = 0.73, slope = 81.9 $\mathrm{ppbv\,ppbv^{-1}}$, n = 1034) and was highest (together with HCN) in the Chinese urban plumes (Figure 5, bottom panel), implying an anthropogenic source. Thus we find no convincing evidence of a biogenic source of nitriles and do not include such a source in our simulations.

4. Simulation of Observations

We examine in this section how the global specification of sources and sinks of HCN and CH_3CN presented in section 3 allows a successful simulation of the TRACE-P observations and what constraints this successful simulation provides. The model evaluation also considers CO, since our source specifications for HCN and CH_3CN are based on relationships with CO. We also examine the consistency of our simulation with the global data sets of HCN columns previously used as constraints by *Li et al.* [2000] and with the INDOEX data of *de Laat et al.* [2001].

As a general assessment of our simulation, we show in Figure 6 the frequency distributions of the observed and simulated HCN, CH_3CN, and CO concentrations along the ensemble of TRACE-P flight tracks. The simulated mean and median values agree with the observed values to within 10 pptv for HCN, 5 pptv for CH_3CN, and 5 ppbv for CO. There are no systematic biases or obvious anomalies in the simulated frequency distributions. Figure 7 shows scatterplots of simulated versus observed concentrations of HCN and CH_3CN for the ensemble of TRACE-P data. The bulk of the points are strongly correlated, but the correlations are much smaller at high mixing ratios (primarily in the boundary layer), likely because of model errors in the location of plumes. For further evaluation of the simulation we examine vertical distributions and correlations between species.

4.1. Vertical Distributions

The observed and simulated vertical profiles of HCN, CH_3CN, and CO for the ensemble of TRACE-P measurements are shown in Figure 1. The model reproduces the increase of CO mixing ratios and decrease of HCN and CH_3CN mixing ratios from the free troposphere to the MBL. For the background conditions over the NW Pacific (Figure 2), the model reproduces the gradients between the free troposphere and the MBL driven by ocean uptake. Also shown in Figure 1 are the relative contributions from biomass burning and residential coal burning simulated in the model using tagged tracers. Biomass burning accounts for 70-85% of total HCN and 90-95% of total CH_3CN in the free troposphere (above 2 km), while in the boundary layer the fractions are 45% and 75%, respectively. Thus both gases can be used as tracers of biomass burning in the free troposphere, but not in the boundary layer. Simulated and observed mean vertical profiles of HCN and CH_3CN show enhancements at 2-4 and 8-11 km (Figure 1). These correspond to preferential altitudes for frontal and convective outflow of

biomass burning pollution, respectively [*Bey et al.*, 2001b; *Liu et al.*, 2002].

We also compare model results in Figure 8 to aircraft measurements of CH_3CN made over the northern Indian Ocean during the INDOEX campaign [*de Laat et al.*, 2001]. In contrast to TRACE-P, the INDOEX observations show maximum concentrations in the MBL due to boundary layer outflow from the Indian subcontinent associated with the winter-spring monsoon. The model reproduces this enhancement, demonstrating that it is consistent with our representation of the ocean sink.

4.2. Correlations Between HCN, CH_3CN, and CO

Figures 9a and 9b compares the observed and simulated correlations between HCN, CH_3CN, and CO for the ensemble of the TRACE-P data in the free troposphere and the boundary layer. The model reproduces the slopes of the correlations to within their errors both in the biomass burning plumes in the free troposphere (Figure 9a) and in the boundary layer (Figure 9b). Differences in slopes between the free troposphere and the boundary layer reflect the dominant influence of biomass burning in the free troposphere, and the added influence from the urban source (residential coal burning) and the deposition sink in the MBL. The CH_3CN-CO correlation is poor in the boundary layer ($r = 0.29$ in the observations and $r = 0.24$ in the model), while the HCN-CO correlation is strong ($r = 0.85$ in the observations and $r = 0.77$ in the model), reflecting the consistency between the urban and biomass burning emission ratios for HCN/CO but the much lower urban ratios for CH_3CN/CO. The CH_3CN-CO relationship in the boundary layer shows two branches, both in the model and in the observations, reflecting (1) the subsidence of biomass burning influence from the free troposphere (high CH_3CN, low CO), and (2) the urban outflow influence (low CH_3CN, high CO).

4.3. HCN Columns

Spectroscopic measurements of HCN atmospheric columns were made at three Japanese sites during TRACE-P as part of a long-term observational program [*Zhao et al.*, 2000, 2002]. The three sites are Moshiri (44°N, 142°E, 0.28 km altitude), Rikubetsu (43.5°N, 144°E, 0.37 km altitude), and Tsukuba (36°N, 140°E, 0.03 km altitude). The data for the TRACE-P period are shown in Figure 10a (solid circles). The columns at Tsukuba show much higher variation than at Moshiri and Rikubetsu, reflecting the latitudinal difference and the proximity of Tsukuba to the main channel of Asian outflow at 25-35°N [*Bey et al.*, 2001b; *Liu et al.*,

this issue]. The increases in the columns from February to April are consistent with the previous observation of a spring-summer HCN column maximum at these sites [*Zhao et al.*, 2000, 2002], and can be explained by the seasonal variation of biomass burning emissions [*Li et al.*, 2000].

Figure 10 compares model results for the TRACE-P period with HCN columns at three Japanese sites. HCN columns were retrieved from solar infrared spectra, and the averaging kernel and *a priori* vertical profile from the retrievals [*Zhao et al.*, 2000, 2002] were applied to the model results. The HCN columns average 4×10^{15} molecules cm^{-2} with high values of $5-7 \times 10^{15}$ molecules cm^{-2}, both in the observations and the model, consistent with previous column measurements at northern middle latitudes [*Mahieu et al.*, 1995, 1997; *Zhao et al.*, 2000, 2002]. A scatterplot of simulated versus observed HCN columns is shown in Figure 11. There is strong correlation (r = 0.82), reflecting in part the seasonal increase from February to April (Figure 12), and no significant bias.

Multi-year measurements of HCN columns are available from several sites in the northern hemisphere and provide another important test for the model. Figure 11 compares the seasonal variations in these multi-year records, including data from the Japanese sites [*Zhao et al.*, 2000, 2002], Kitt Peak in Arizona [*Mahieu et al.*, 1995], Jungfraujoch in the Swiss Alps [*Mahieu et al.*, 1995, 1997], and Ny Ålesund in Spitsbergen [*Li et al.*, 2000], to model results for 2000. Observations for 1998 were excluded because of anomalous fire influence throughout the northern hemisphere [*Rinsland et al.*, 1999, 2000; *Zhao et al.*, 2002].

The observed spring-summer maxima observed are due to biomass burning in the northern tropics in winter-spring, with a phase lag from meridional transport and augmented by forest fires at middle and high latitudes in summer [*Li et al.*, 2000]. The good simulation of the relative seasonal amplitude constrains the lifetime of HCN and is consistent with the dominance of the ocean sink. The May-July maxima at the Japanese sites are due to fires in Mongolia and northern China that are present in all years of the record *Zhao et al.* [2000, 2002].

5. Global Budgets and Distributions of HCN and CH_3CN

The global atmospheric budgets of HCN and CH_3CN from the model are shown in Table 2. Biomass burning contributes 0.63 Tg N yr^{-1} to global HCN and 0.47 Tg N yr^{-1} to global CH_3CN, while the corresponding sources from residential coal burning are 0.2 and

0.03 $\mathrm{Tg\,N\,yr^{-1}}$, respectively. Ocean uptake dominates the loss of both HCN (0.73 $\mathrm{Tg\,N\,yr^{-1}}$) and CH_3CN (0.36 $\mathrm{Tg\,N\,yr^{-1}}$), while the sink from reaction with OH is relatively small (0.1 $\mathrm{Tg\,N\,yr^{-1}}$ for HCN and 0.13 $\mathrm{Tg\,N\,yr^{-1}}$ for CH_3CN). The resulting tropospheric lifetimes are 5.3 months for HCN and 5.8 months for CH_3CN. Our HCN lifetime is longer, and the implied global source smaller, than the constraints derived in our previous work from the observed relative seasonal variation of HCN columns [*Li et al.*, 2002, Table 1]. However, the present simulation does not seem incompatible with the observed columns (Figure 12).

Figures 13 shows simulated monthly mean concentrations of HCN and CH_3CN in April 2001. Surface concentrations are maximum over biomass burning regions in SE Asia, central America, and central Africa ($>$ 1000 pptv). Surface concentrations are very low ($<$ 50 pptv) at high southern latitudes, reflecting the remoteness from sources and the sink from ocean uptake under our assumption of uniform saturation ratio. Observations in this part of the world are evidently needed. Concentrations in the middle troposphere at 500 hPa are highest over SE Asia and downwind, with a band of relatively high concentrations ($>$ 200 pptv for HCN) at 5-40°N, due to biomass burning influence.

6. Conclusions

We used a global 3-D model analysis of in situ HCN-CH_3CN-CO aircraft observations made over the North Pacific during the TRACE-P aircraft mission (February-April 2001) to improve understanding of the atmospheric budgets of both gases. Vertical gradients of HCN and CH_3CN observed in remote marine air confirm the previous hypotheses of a dominant ocean sink for HCN [*Li et al.*, 2000] and CH_3CN [*Hamm and Warneck*, 1990]. Following *Singh et al.* [this issue], we used these gradients to derive deposition velocities of 0.13 $\mathrm{cm\,s^{-1}}$ for both gases, corresponding to saturation ratios of 0.79 for HCN and 0.88 for CH_3CN. These deposition velocities imply lifetimes of three months for $\mathrm{HCN(aq)/CN^-}$ and 14 months for $\mathrm{CH_3CN(aq)/CN^-}$ against consumption in the oceanic mixed layer.

Observations from TRACE-P in biomass burning plumes from SE Asia confirmed the importance of biomass burning as a global source for HCN and CH_3CN, while observations in southern California confirmed that automobile exhaust is not a significant source for either gas [*Singh et al.*, this issue]. However, HCN and CH_3CN observed in fresh Chinese urban plumes indicate emissions of anthropogenic origin with a much higher HCN/CH_3CN ratio than from biomass burning. We tentatively attribute these enhancements to residential coal burning.

We use in our global model biomass burning and residential coal burning emission ratios relative to CO of 0.27% and 1.6% respectively for HCN, and 0.2% and 0.25% respectively for CH_3CN, as providing the best fit to the TRACE-P observations within the constraints offered by the HCN-CH_3CN-CO relationships observed in biomass burning and urban plumes. It also offers a good simulation of observed HCN columns, both during TRACE-P and over the multi-year record, and of CH_3CN vertical distributions over the northern Indian Ocean. The resulting simulation captures the observed frequency distributions of HCN and CH_3CN, their vertical distributions, and their correlations with CO.

Our global budgets of HCN and CH_3CN indicate biomass burning sources of 0.63 and 0.47 $\mathrm{Tg\,N\,yr^{-1}}$, respectively, and residential coal burning sources of 0.2 and 0.03 $\mathrm{Tg\,N\,yr^{-1}}$, respectively. Ocean uptake is the dominant sink for both; oxidation by OH is an additional minor sink. The resulting tropospheric lifetimes are 5.3 months for HCN and 5.8 months for CH_3CN. The HCN lifetime is longer, and the global source smaller, than in our previous model analysis [*Li et al.*, 2000], but it still provides an unbiased simulation of the relative seasonal cycle of HCN columns which was the main constraint in that previous analysis. The model predicts maximum surface air concentrations of HCN and CH_3CN over biomass burning regions and very low (< 50 pptv) concentrations at high southern latitudes due to ocean uptake under the assumption of a uniform saturation ratio. Observations are evidently needed to test this assumption. Concentrations in the middle troposphere are highest over tropical biomass burning regions and downwind, with a band of high concentrations at 5-40°N, due to biomass burning influence. The dominance of biomass burning as a source of both gases in the free troposphere (70-85% for HCN and 90-95% for CH_3CN) in TRACE-P implies that they can be used there as biomass burning tracers. However, more work is needed to characterize the nature of the Chinese urban source observed in TRACE-P.

Acknowledgments. Discussions with Jennifer Logan and Rose Yevich were very helpful. This work was funded by the Atmospheric Chemistry Program of the U.S. National Science Foundation and by the NASA Global Tropospheric Chemistry Program.

References

Andreae, M. O., and P. Merlet, Emission of trace gases and aerosols from biomass burning, *Global Biogeochem. Cycles, 15,* 955-966, 2001.

Asher, W., The sea-surface microlayer and its effect on global air-sea gas transfer, in *The Sea Surface and Global Change,* edited by P. S. Liss and R. A. Duce, Cambridge University Press, Cambridge, UK, 1997.

Bange, H. W., and J. Williams, New directions: Acetonitrile in atmospheric and biogeochemical cycles, *Atmos. Environ., 34,* 4959-4960, 2000.

Bertschi, I. et al., The trace gas and particle emissions from fires in large-diameter and belowground biomass fuels, *J. Geophys. Res.*, submitted, 2002.

Bey, I. et al., Global modeling of tropospheric chemistry with assimilated meteorology: Model description and evaluation, *J. Geophys. Res., 106,* 23,073-23,095, 2001a.

Bey, I., D. J. Jacob, J. A. Logan, and R. M. Yantosca, Asian chemical outflow to the Pacific: Origins, pathways and budgets, *J. Geophys. Res., 106,* 23,097-23,113, 2001b.

Blake, N. et al., Large-scale latitudinal and vertical distributions of NMHCs and selected halocarbons in the troposphere over the Pacific Ocean during the March-April 1999 Pacific Exploratory Mission (PEM-Tropics B), *J. Geophys. Res., 106,* 32,627-32,644, 2001.

Brasseur, G., E. Arijs, A. de Rudder, D. Nevejans, and J. Ingels, Acetonitrile in the atmosphere, *Geophys. Res. Lett., 10,* 725-728, 1983.

Carmichael, G. R. et al., Regional-scale chemical transport modeling in support of intensive field experiments: Overview and analysis of the TRACE-P observations, *J. Geophys. Res.,* this issue, 2002.

Chan, L. Y., C. Y. Chan, H. Y. Liu, S. A. Christopher, S. J. Oltmans, and J. M. Harris, A case study on the biomass burning in southeast Asia and enhancement of tropospheric ozone over Hong Kong, *Geophys. Res. Lett., 27,* 1479-1482, 2000.

Cicerone, R. J., and R. Zellner, The atmospheric chemistry of hydrogen cyanide (HCN), *J. Geophys. Res., 88,* 10,689-10,696, 1983.

Crutzen, P. J., and M. O. Andreae, Biomass burning in the tropics: Impact on atmospheric chemistry and biogeochemical cycles, *Science, 250,* 1669-1678, 1990.

de Fré, R., P. Bruynseraede, and J. Kretzschmar, Air pollution measurements in traffic tunnels, *Environ. Health Perspect., 102,* Suppl. 4, 1994.

de Gouw, J. A., C. Warneke, D. D. Parrish, J. S. Holloway, M. Trainer, F. C. Fehsenfeld, Emission sources and ocean uptake of acetonitrile (CH_3CN) in the atmosphere, *J. Geophys. Res.,* manuscript in preparation, 2002.

DeMore, W. B. et al., Chemical kinetics and photochemical data for use in stratospheric modeling, *JPL Publ. 97-4,* 1997.

de Laat, A. T. J., J. A. de Gouw, J. Lelieveld, and A. Hansel, Model analysis of trace gas measurements and pollution impact during INDOEX, *J. Geophys. Res., 106,* 28,469-28,480, 2001.

Dulson, W., Organisch-chemische Fremdstoffe in atmosphärischer Luft, in *Schriftenreihe des Vereins für Wasser, Boden und Lufthygiene,* vol. 47, edited by A. Heller, Gustav Fischer Verlag, Stuttgart, Federal Repulic of Germany, 1978.

Duncan, B. N., J. A. Logan, I. Bey, R. V. Martin, D. J. Jacob, and R. M. Yantosca, Model study of the variability and trends of carbon monoxide (1988-1997) 1. Model formulation, evaluation, and sensitivity, *J. Geophys. Res.,* in press, 2002.

Fall, R., S. Kato, and V. M. Bierbaum, New directions: The biogenic acetone-HCN connection, *Atmos. Environ., 35,* 1713-1714, 2001.

Flagan, R. C., and J. H. Seinfeld, *Fundamentals of Air Pollution Engineering,* Chap. 3, Prentice Hall, Englewood Cliffs, NJ, 1988.

Fritz, B., K. Lorenz, W. Steinert, and R. Zellner, Rate of oxidation of HCN by OH radicals at lower temperatures, *Oxid. Commun., 6,* 363-370, 1984.

Goode, J. G. et al., Measurements of excess O_3, CO_2, CO, CH_4, C_2H_4, C_2H_2, HCN, NO, NH_3, HCOOH, CH_3COOH, HCHO, and CH_3OH in 1997 Alaskan biomass burning plumes by Airborne Fourier Transform Infrared Spectroscopy (AFTIR), *J. Geophys. Res., 105,* 22,147-22,166, 2000.

Hamm, S., and P. Warneck, The interhemispheric distribution and the budget of acetonitrile in the troposphere, *J. Geophys. Res., 95,* 20,593-20,606, 1990.

Heald, C. L. et al., Biomass burning emission inventory with daily resolution: Application to aircraft observations of Asian outflow, *J. Geophys. Res.,* this issue, 2002.

Heikes, B. et al., Ozone, hydroperoxides, oxides of nitrogen, and hydrocarbon budgets in the marine boundary layer over the South Atlantic, *J. Geophys. Res., 101,* 24,221-24,234, 1996.

Heikes, B. et al., Atmospheric methanol budget and ocean implication, *J. Geophys. Res.,* submitted, 2002.

Holzinger, R. et al., Biomass burning as a source of formaldehyde, acetaldehyde, methanol, acetone, acetonitrile, and hydrogen cyanide, *Geophys. Res. Lett., 26,* 1161-1164, 1999.

Holzinger, R., A. Jordan, A. Hansel, and W. Lindinger, Automobile emissions of acetonitrile: Assessments of its contribution to the global source, *Atmos. Environ., 38,* 187-193, 2001.

Hurst, D. F., D. W. T. Griffith, and G. D. Cook, Trace gas emissions from biomass burning in tropical Australian savannas, *J. Geophys. Res., 99,* 16,441-16,456, 1994a.

Hurst, D. F. D. W. T. Griffith, J. N. Carras, D. J. Williams, and P. J. Fraser, Measurements of trace gases emitted by Australian savanna fires during the 1990 dry season, *J. Atmos. Chem., 18,* 33-56, 1994b.

Jacob, D. J. et al., The transport and chemical evolution over the Pacific (TRACE-P) mission: Design, execution, and overview of results, *J. Geophys. Res.,* this issue, 2002.

Kara, A. B., P. A. Rochford, and H. E. Hurlburt, Mixed layer depth variability and barrier layer formation over the North Pacific Ocean, *J. Geophys. Res., 105,* 16,783-16,801, 2000.

Lenschow, D. H., R. Pearson Jr., and B. B. Stankov, Measurements of ozone vertical flux to ocean and forest, *J. Geophys. Res., 87,* 8833-8837, 1983.

Li, Q., D. J. Jacob, I. Bey, R. M. Yantosca, Y. Zhao, Y. Kondo, and J. Notholt, Atmospheric hydrogen cyanide (HCN): Biomass burning source, ocean sink? *Geophys. Res. Lett., 27,* 357-360, 2000.

Li, Q. et al., Transatlantic transport of pollution and its effects on surface ozone in Europe and North America, *J. Geophys. Res.,* 107(D13), 10.1029/2001JD001422, 2002.

Liss, P. S., and P. G. Slater, Flux of gases across the air-sea interface, *Nature, 247,* 181-184, 1974.

Liu, H., W. L. Chang, S. J. Oltmans, L. Y. Chan, and J. M. Harris, On springtime high

ozone events in the lower troposphere from southeast Asian biomass burning, *Atmos. Environ., 33,* 2403-2410, 1999.

Liu, H., D. J. Jacob, I. Bey, R. M. Yantosca, B. N. Duncan, and G. W. Sachse, Transport pathways for Asian combustion outflow over the Pacific: Interannual and seasonal variations, *J. Geophys. Res.,* this issue, 2002.

Lobert, J. M., Combustion of plant biomass as a source of atmospheric trace gases: Cyano compounds, CO, CO_2, and NO_x, Ph.D. thesie, University of Mainz, Germany, 1989.

Lobert, J. M., D. H. Scharffe, W. M. Hao, and P. J. Crutzen, Importance of biomass burning in the atmospheric budgets of nitrogen-containing gases, *Nature, 346,* 552-554, 1990.

Lobert, J. M. et al., Experimental evaluation of biomass burning emissions: Nitrogen and carbon containing compounds, in *Global Biomass Burning: Atmospheric, Climatic and Biospheric Implications,* pp. 289-304, edited by J. S. Levine, MIT Press, Cambridge, Mass., 1991.

Mahieu, E., C. P. Rinsland, R. Zander, P. Demoulin, L. Delbouille, and G. Roland, Vertical column abundances of HCN deduced from ground-based infrared solar spectra: Long-term trend and variability, *J. Atmos. Chem., 20,* 299-310, 1995.

Mahieu, E., R. Zander, L. Delbouille, P. Demoulin, G. Roland, and C. Servais, Observed trends in total vertical column abundances of atmospheric gases from IR solar spectra recorded at the Jungfraujoch, *J. Atmos. Chem., 28,* 227-243, 1997.

Marland, G., R. Andres, T. Boden, C. Johnston, and A. Brenkert, Global, regional, and national CO_2 emission estimates from fossil-fuel burning, hydraulic cement production, and gas flaring: 1751-1995, *CDIAC-Database* NDP-030/R8, http://cdiac.esd.ornl.gov/ndps/ndp030.html, 1998.

Nightingale, P. D. et al., In situ evaluation of air-sea gas exchange parameterizations using novel conservative and volatile tracers, *Global Biogeochem. Cycles, 14,* 373-387, 2000.

Olivier, J., and J. Berdowski, Global emissions sources and sinks, in *The Climate System,* edited by J. Berdowski, R. Guicherit, and B. Heij, pp. 33-78. A. A. Balkema Publishers/Swets & Zeitlinger Publishers, Lisse, The Netherlands, 2001.

Rinsland, C. P. et al., Infrared solar spectroscopic measurements of free tropospheric CO, C_2H_6, and HCN above Mauna Loa, Hawaii: Seasonal variations and evidence for

enhanced emissions from the southeast Asian tropical fires of 1997-1998, *J. Geophys. Res., 104*, 18,667-18,680, 1999.

Rinsland, C. P., E. Mahieu, R. Zander, P. Demoulin, J. Forrer, and B. Buchmann, Free tropospheric CO, C_2H_6, and HCN above central Europe: Recent measurements from the Jungfraujoch station including the detection of elevated columns during 1998, *J. Geophys. Res., 105*, 24,235-24,249, 2000.

Rinsland, C. P., A. Goldman, R. Zander, and E. Mahieu, Enhanced tropospheric HCN columns above Kitt Peak during the 1982-1983 and 1997-1998 El Ninõ warm phases, *J. Quant. Spectrosc. Radiat. Transfer., 609*, 3-8, 2001.

Rinsland, C. P. et al., Multiyear infrared solar spectroscopic measurements of HCN, CO, C_2H_6, and C_2H_2 tropospheric columns above Lauder, New Zealand (45°S latitude), *J. Geophys. Res.*, 107(D13), 10.1029/2001JD001150, 2002.

Sander, R., Compilation of Henry's law constants for inorganic and organic species of potential importance in environmental chemistry (version 3), http://www.mpch-mainz.mpg.de/~sander/res/henry.html.

Seiler, W., and P. J. Crutzen, Estimates of gross and net fluxes of carbon between the biosphere and the atmosphere from biomass burning, *Climate Change*, *2*, 207-247, 1980.

Singh, H. et al., In situ measurements of HCN and CH_3CN in the Pacific troposphere: Sources, sinks, and comparisons with spectroscopic observations, *J. Geophys. Res.*, this issue, 2002.

Streets, D. et al., An inventory of gaseous and primary aerosol emissions in Asia in the year 2000, *J. Geophys. Res.*, this issue, 2002.

Warneke, C., and J. A. de Gouw, Organic trace gas composition of the marine boundary layer over the northwest Indian Ocean in April 2000, *Atmos. Environ., 35*, 5923-5933, 2001.

Williams, J. et al., An atmospheric chemistry interpretation of mass scans obtained from a Proton Transfer Mass Spectrometer flown over the tropical rainforest of Surinam, *J. Atmos. Chem., 38*, 133-166, 2001.

Wine, P., R. Strekowski, J. Nicovich, M. McKee, G. Chen, and D. Davis, Atmospheric chemistry of HCN, paper PHYS 134, 224rd ACS National Meeting, Boston, MA, 2002.

Yokelson, R. J., R. Susott, D. E. Ward, J. Reardon, and D. W. T. Griffith, Emissions from smoldering combustion of biomass measured by open-path Fourier transform infrared spectroscopy, *J. Geophys. Res., 102,* 18,865-18,877, 1997.

Yokelson, R. J. et al., Emissions of formaldehyde, acetic acid, methanol, and other trace gases from biomass fires in North Carolina measured by Airborne Fourier Transform Infrared Spectroscopy (AFTIR), *J. Geophys. Res., 104,* 30,109-30,125, 1999.

Yokelson, R. J., I. T. Bertschi, T. J. Christian, P. V. Hobbs, D. E. Ward, and W. M. Hao, An overview of trace gas measurements in nascent, aged, and cloud-processed smoke from African savanna fires by airborne Fourier Transform Infrared Spectroscopy (AFTIR), *J. Geophys. Res.,* submitted, 2002.

Zhao, Y. et al., Seasonal variations of HCN over northern Japan measured by ground-based infrared solar spectroscopy, *Geophys. Res. Lett., 27,* 2085-2088, 2000.

Zhao, Y. et al., Spectroscopic measurements of tropospheric CO, C_2H_6, C_2H_2, and HCN in northern Japan, *J. Geophys. Res.,* 107(D18), 10.1029/2001JD000748, 2002.

Received _____

Figure Captions

Figure 1. Vertical distributions of of HCN, CH_3CN, and CO for the ensemble TRACE-P data over the North Pacific. Individual observations are shown as dots. Solid circles, triangles, and horizontal bars represent means, medians, and standard deviations, respectively.

Figure 2. Vertical distributions of HCN and CH_3CN observed in TRACE-P over the North Pacific under background conditions (CO < 120 ppbv and $C_2Cl_4 < 10$ pptv). Individual observations are shown as dots. Solid circles, triangles, and horizontal bars represent means, medians, and standard deviations, respectively.

Figure 3. Observed HCN (solid circles) and CH_3CN (open circles) correlations with CO in three Chinese urban plumes sampled during TRACE-P (DC-8 flights 9, 12, and 13) below 2 km altitude. Regression lines (RMA method) are also shown.

Figure 4. Observed CH_3CN:HCN correlations in plumes sampled during TRACE-P. Solid circles: sampled at 8-11 km on DC-8 flights 4, 7, 9, 12, 13, 14, 15, 17, 18, and 19; plumes at that altitude were largely devoid of anthropogenic influence [*Liu et al.*, this issue]. Open circles: Chinese urban plumes below 2 km (DC-8 flights 9, 12, and 13). Regression lines are shown.

Figure 5. Observed HCN and CO correlations with Methanol for the ensemble of TRACE-P data. Regression lines are shown.

Figure 6. Frequency distributions of observed (solid line) and simulated (dashed line) mixing ratios of HCN, CH_3CN, and CO for the ensemble TRACE-P data over the North Pacific.

Figure 7. Scatterplots of simulated versus observed mixing ratios of HCN and CH_3CN for the ensemble of TRACE-P data. The 1:1 line is also shown.

Figure 8. Vertical distribution of CH_3CN concentrations over the northern Indian ocean in March 2001. Median aircraft observations from the INDOEX campaign [*de Laat et al.*, 2001] are shown as symbols with standard deviations. Monthly mean model results for the corresponding month and region (0-10°N, 65-80°E) are shown as the solid line.

Figure 9a. Observed and simulated HCN-CH_3CN-CO correlations in the free troposphere (above 2 km) during TRACE-P. Regression lines and correlation coefficients are shown.

Figure 9b. Same as Figure 9a but the boundary layer (below 2 km).

Figure 10. Time series of observed (solid circles) and simulated (open circles) 24-hour average HCN columns (molecules cm^{-2}) at the three Japanese stations of Moshiri (44°N, 142°E, 0.28 km altitude), Rikubetsu (43.5°N, 144°E, 0.37 km altitude), and Tsukuba (36°N, 140°E, 0.03 km altitude) during TRACE-P (February-April 2001).

Figure 11. Scatter plot of observed and simulated daily HCN columns (molecules cm^{-2}) at Moshiri, Rikubetsu, and Tsukuba in TRACE-P. Values are averages over the three sites. The regression line is calculated without the outlier.

Figure 12. Monthly mean HCN total columns (molecules cm^{-2}) retrieved from spectroscopic measurements at Moshiri and Rikubetsu in Japan [*Zhao et al.*, 2000, 2002], Kitt Peak in Arizona [*Mahieu et al.*, 1995], Jungfraujoch in the Swiss Alps [*Mahieu et al.*, 1995, 1997], and Ny Ålesund in Spitsbergen [*Li et al.*, 2000]. Data for the two Japanese sites are monthly means and vertical bars indicate standard deviations. The solid lines represent simulated daily average HCN total columns for 2000.

Figure 13. Simulated monthly mean concentrations of HCN and CH_3CN in surface air and at 500 hPa for April 2001.

Table 1. Global HCN and CH_3CN source estimates (unit: $Tg\,N\,yr^{-1}$)

	Biomass burning	Biofuels	Car exhaust	Residential coal	Biogenic	Total	References
HCN							
						0.2	*Cicerone and Zellner* [1983][a]
	0.37-1.89						*Lobert et al.* [1990][b]
	0.64-3.18		0.04				*Lobert et al.* [1991][c]
	0.1-0.3						*Holzinger et al.* [1999][d]
	1.4-2.9					1.4-2.9	*Li et al.* [2000][e]
	0.26	0.21				0.47	*Andreae and Merlet* [2001][f]
	0.7-0.9		<0.02		0.2	1.1	*Singh et al.*[this issue][g]
	0.63			0.2		0.83	this work[h]
CH_3CN							
	0.27		0.09			0.36	*Hamm and Warneck* [1990][i]
	0.14-0.75						*Lobert et al.* [1990][b]
	0.23-1.13						*Lobert et al.* [1991][c]
	0.14-0.34		0.01				*Holzinger et al.* [1999, 2001][d]
	0.27	0.17				0.44	*Andreae and Merlet* [2001][f]
						0.44	*de Laat et al.* [2001][j]
	0.4-0.5		<0.02		0.2	0.7	*Singh et al.*[this issue][g]
	0.47			0.03		0.5	this work[h]

[a]Source needed to balance the global sink from reaction of HCN with OH. However, we now know that this reaction makes only a small contribution to the total HCN sink [*Li et al.*, 2000].

[b]Based on emission factors per unit nitrogen of $2.42 \pm 1.79\%$ for HCN and $0.95 \pm 0.74\%$ for CH_3CN measured in laboratory biomass burning experiments, and a global biomass burning nitrogen volatilization estimate of 24-57 $Tg\,N\,yr^{-1}$ [*Crutzen and Andreae*, 1990]. No detail of the car exhaust source estimate is given.

[c]Based on biomass burning molar emission ratios relative to CO of 1.1% for HCN and 0.25% for CH_3CN measured in laboratory biomass burning experiments, combined with a global biomass burning CO source estimate of 480-860 $Tg\,CO\,yr^{-1}$.

[d]Biomass burning sources based on molar emission ratios (relative to CO) of 0.12% for HCN and 0.13%

for CH_3CN measured in a laboratory biomass burning experiment, combined with a global biomass burning CO source estimate of 210-550 $Tg\,CO\,yr^{-1}$. The automobile exhaust source of CH_3CN is based on a measured CH_3CN molar emission ratio of 0.06 relative to benzene, combined with an emission ratio of 0.6 g benzene per unit fuel (kg C) consumed in traffic [*de Fre et al.*, 1994] and a global fuel consumption estimate of 2.6×10^3 $Tg\,C\,yr^{-1}$ [*Marland et al.*, 1998].

[e]Source needed to balance the HCN loss derived from the relative seasonal amplitude of the column observations, when fitted in a global model simulation (GEOS-CHEM version 3.4) with biomass burning as the only source and ocean uptake as the dominant sink.

[f]Biomass burning sources based on HCN molar emission ratios relative to CO of 0.05% for savanna and grassland and 0.15% for tropical and extratropical forests, and CH_3CN molar emission ratios relative to CO of 0.11% for savanna, grassland, and tropical and extratropical forests. These ratios are combined with a global biomass buring CO source estimate of 480 $Tg\,CO\,yr^{-1}$. Biofuel source estimates are based on molar emission ratios relative to CO of 0.20% for HCN and 0.16% for CH_3CN and a global biofuel CO source estimate of 210 $Tg\,CO\,yr^{-1}$.

[g]Based on biomass burning and biofuel molar emission ratios relative to CO of 0.27% for HCN and 0.15% for CH_3CN, and a global biomass burning CO source estimate of 700 $Tg\,CO\,yr^{-1}$ [*Andreae and Merlet*, 2001]. Additional biogenic sources of 0.2 $Tg\,N\,yr^{-1}$ for both HCN and CH_3CN are invoked to balance estimated global loss rates from ocean uptake.

[h]Global 3-D model study with biomass burning molar emission ratios relative to CO of 0.26% for HCN and 0.15% for CH_3CN and a global biomass burning CO source estimate of 487 $Tg\,CO\,yr^{-1}$ [*Duncan et al.*, 2002]. The residential coal burning source is invoked to explain enhanced HCN and CH_3CN in Chinese urban plumes. It assumes molar emission ratios relative to CO of 1.4% for HCN and 0.5% for CH_3CN and a global residential coal burning CO source of 30 $Tg\,CO\,yr^{-1}$.

[i]The biomass burning source estimate is based on an emission ratio of $2.6 \pm 1.7 \times 10^{-4}$ $g\,CH_3CN\,g\,C^{-1}$ for straw and savannah grass [*Lobert*, 1989] and a global biomass burning carbon source estimate of $3.1 \times 10^3\,Tg\,C\,yr^{-1}$ [*Seiler and Crutzen*, 1980]. The automobile exhaust source estimate is based on a CH_3CN emission factor of 1.3% g/g relative to organic compounds measured in the exhaust of a gasoline-powered engine [*Dulson*, 1978], combined with a global car exhaust source of organic compounds of 21 $Tg\,yr^{-1}$.

[j]Based on biomass burning and biofuel CH_3CN molar emission ratios (relative to CO) of 0.13% [*Holzinger et al.*, 1999] and a global biomass burning and biofuel CO source estimate of 670 $Tg\,CO\,yr^{-1}$.

Table 2. Atmospheric budgets of HCN and CH_3CN

	HCN	CH_3CN
Atmospheric burden (Tg N)	0.43	0.28
Atmospheric lifetime (months)	6.2	6.7
Tropospheric burden(Tg N)[a]	0.37	0.24
Tropospheric lifetime (months)	5.3	5.8
Sources ($Tg\,N\,yr^{-1}$)		
Biomass burning	0.63	0.47
Residential coal burning	0.2	0.03
Sinks ($Tg\,N\,yr^{-1}$)		
Ocean uptake	0.73	0.36
Reaction with OH	0.1	0.14

[a]For the 1000-120 hPa column.

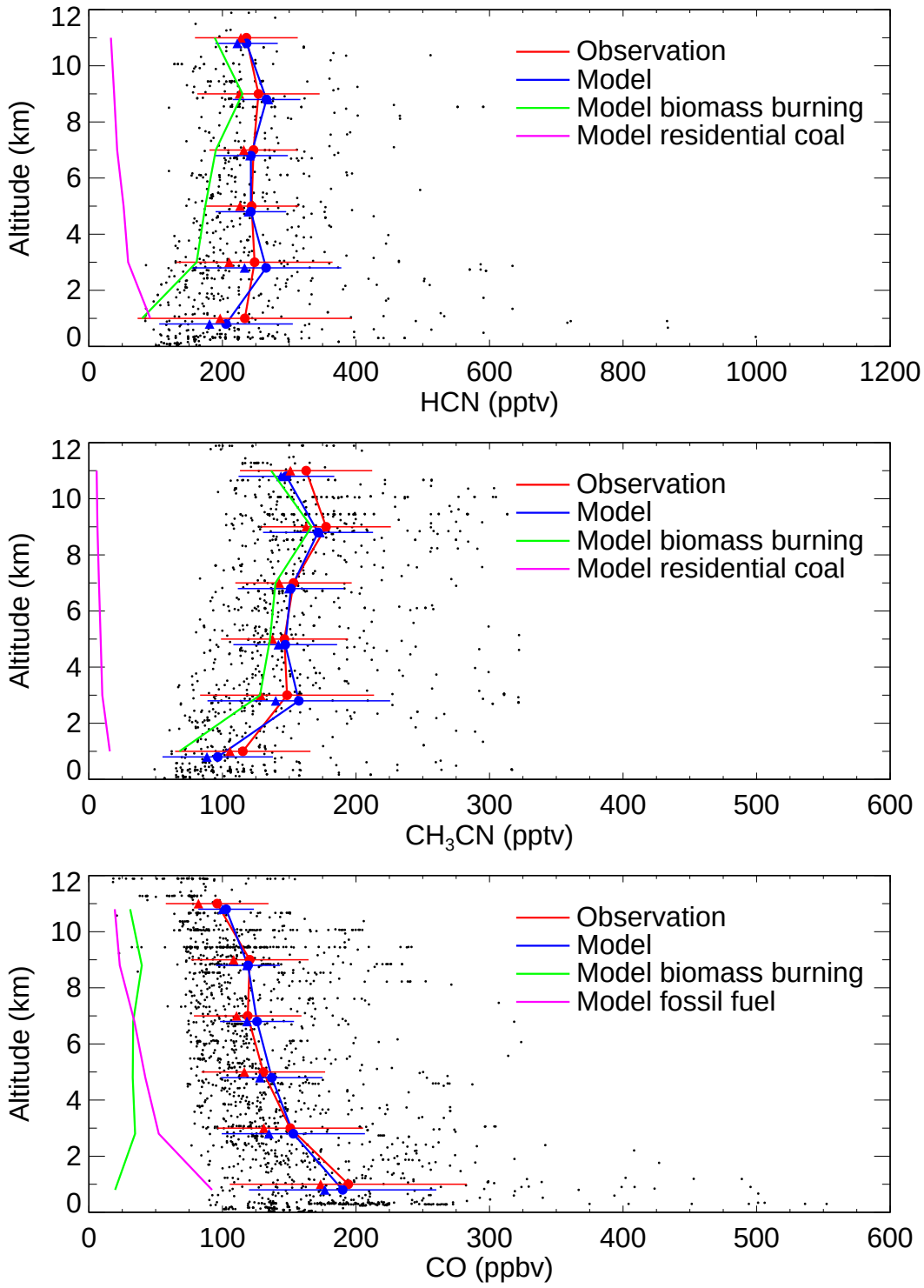

Figure 1. Vertical distributions of of HCN, CH_3CN, and CO for the ensemble TRACE-P data over the North Pacific. Individual observations are shown as dots. Solid circles, triangles, and horizontal bars represent means, medians, and standard deviations, respectively.

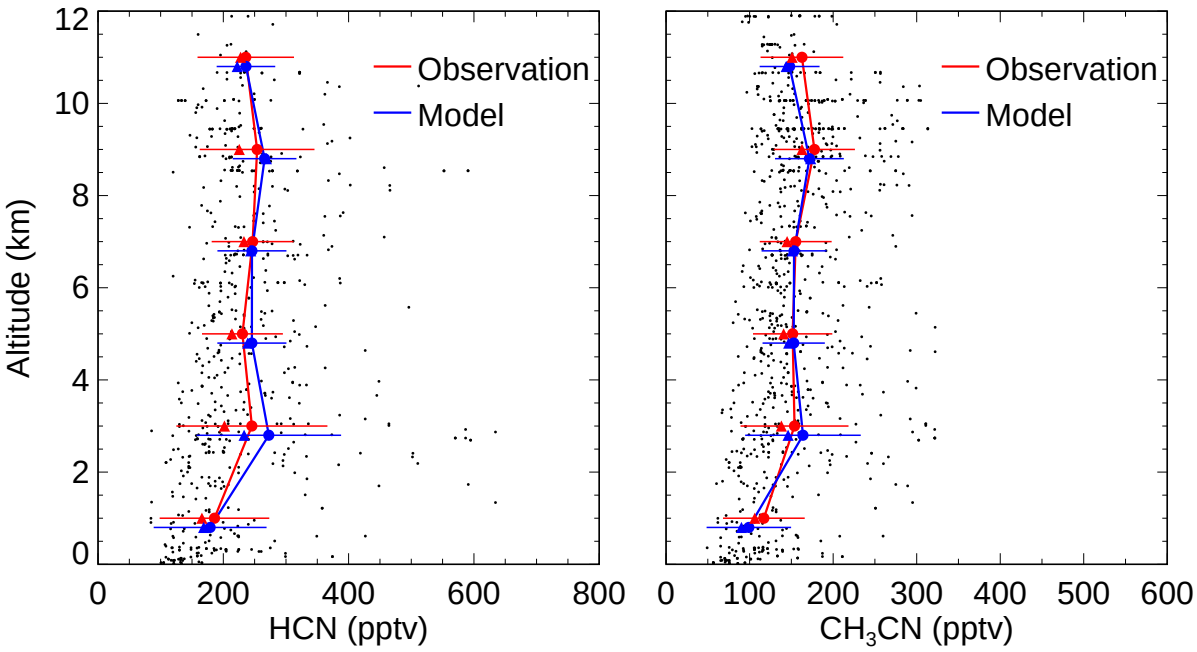

Figure 2. Vertical distributions of HCN and CH_3CN observed in TRACE-P over the North Pacific under background conditions (CO $<$ 120 ppbv and C_2Cl_4 $<$ 10 pptv). Individual observations are shown as dots. Solid circles, triangles, and horizontal bars represent means, medians, and standard deviations, respectively.

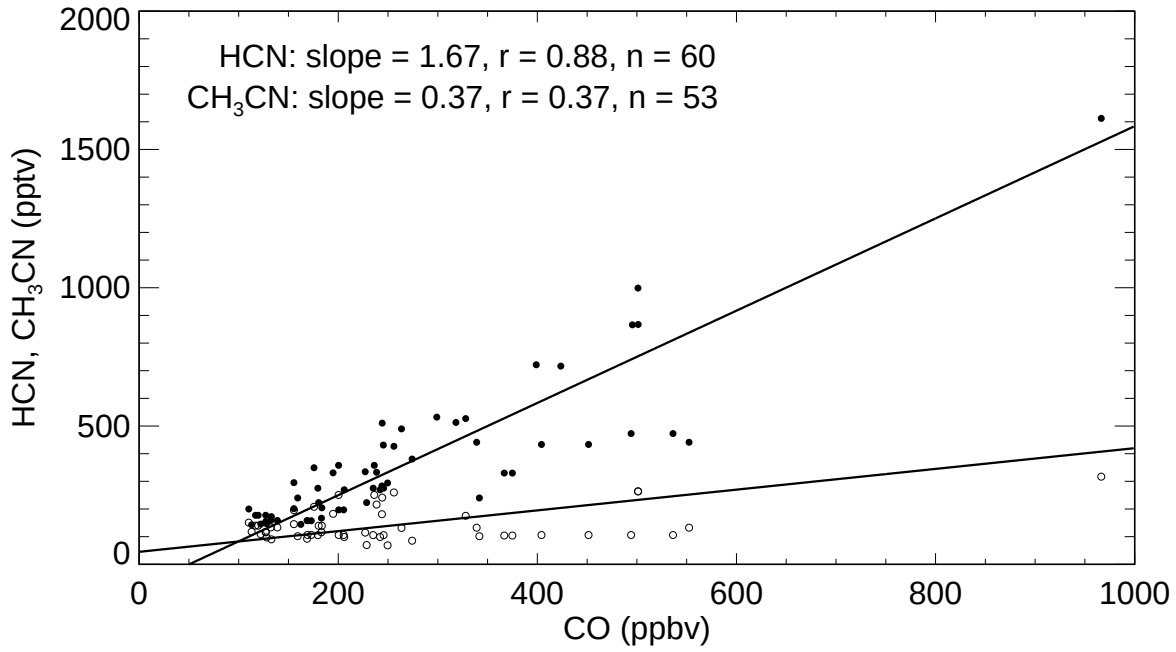

Figure 3. Observed HCN (solid circles) and CH_3CN (open circles) correlations with CO in three Chinese urban plumes sampled during TRACE-P (DC-8 flights 9, 12, and 13) below 2 km altitude. Regression lines (RMA method) are also shown.

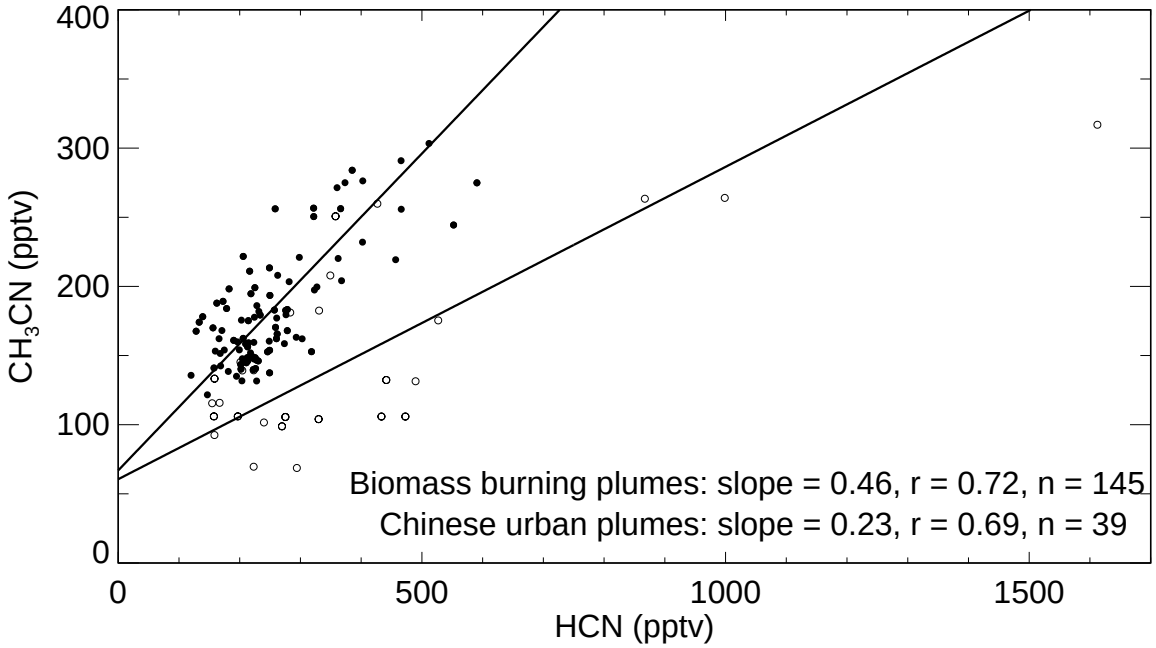

Figure 4. Observed CH_3CN:HCN correlations in plumes sampled during TRACE-P. Solid circles: sampled at 8-11 km on DC-8 flights 4, 7, 9, 12, 13, 14, 15, 17, 18, and 19; plumes at that altitude were largely devoid of anthropogenic influence [*Liu et al.*, this issue]. Open circles: Chinese urban plumes below 2 km (DC-8 flights 9, 12, and 13). Regression lines are shown.

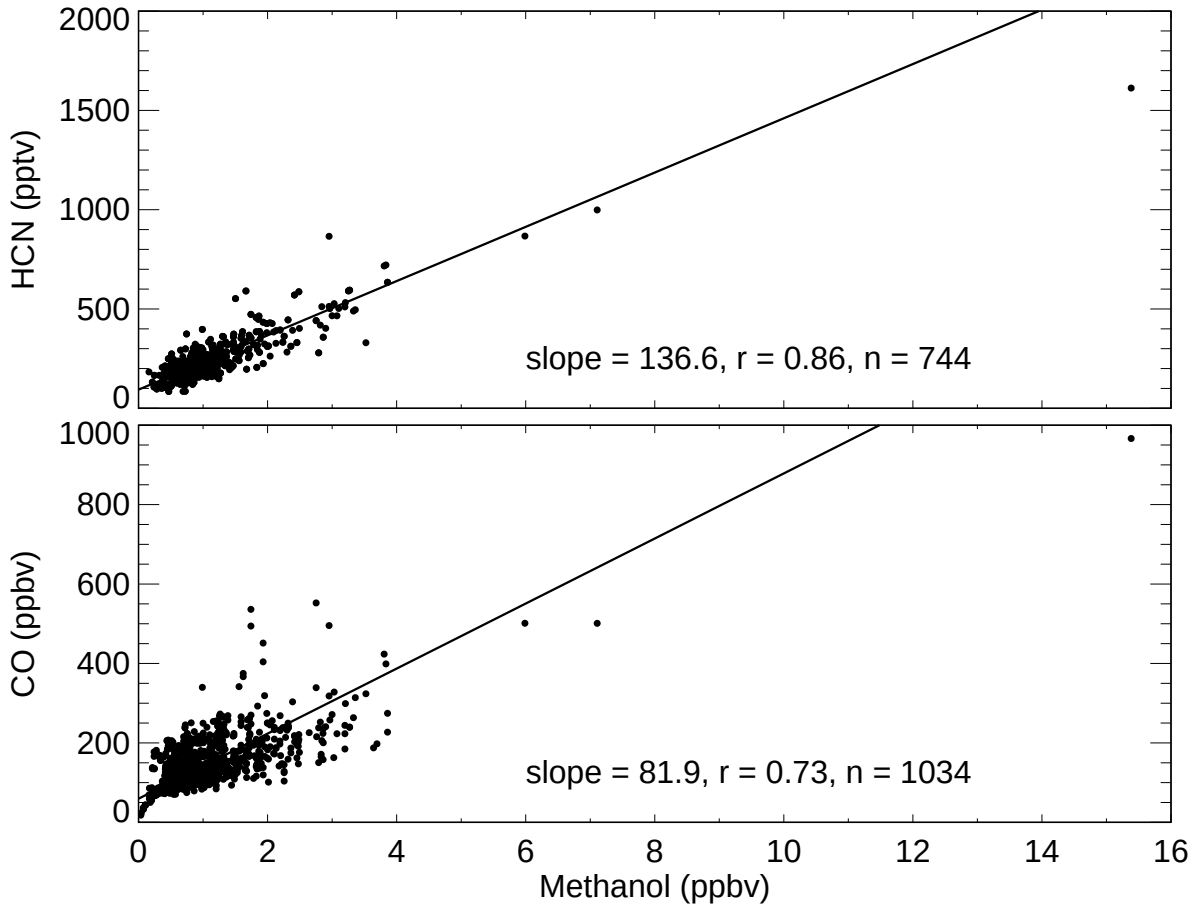

Figure 5. Observed HCN and CO correlations with Methanol for the ensemble of TRACE-P data. Regression lines are shown.

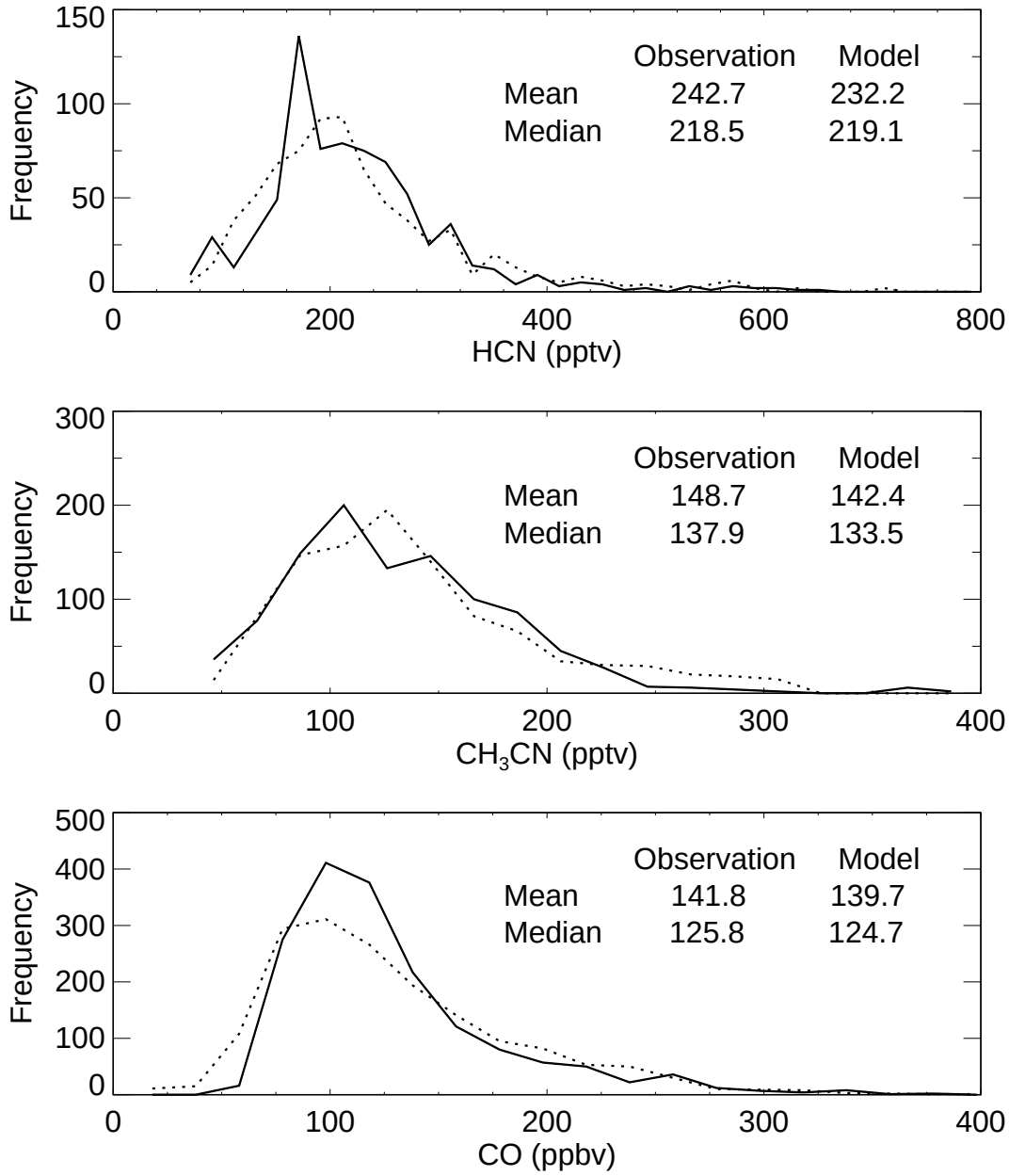

Figure 6. Frequency distributions of observed (solid line) and simulated (dashed line) mixing ratios of HCN, CH_3CN, and CO for the ensemble TRACE-P data over the North Pacific.

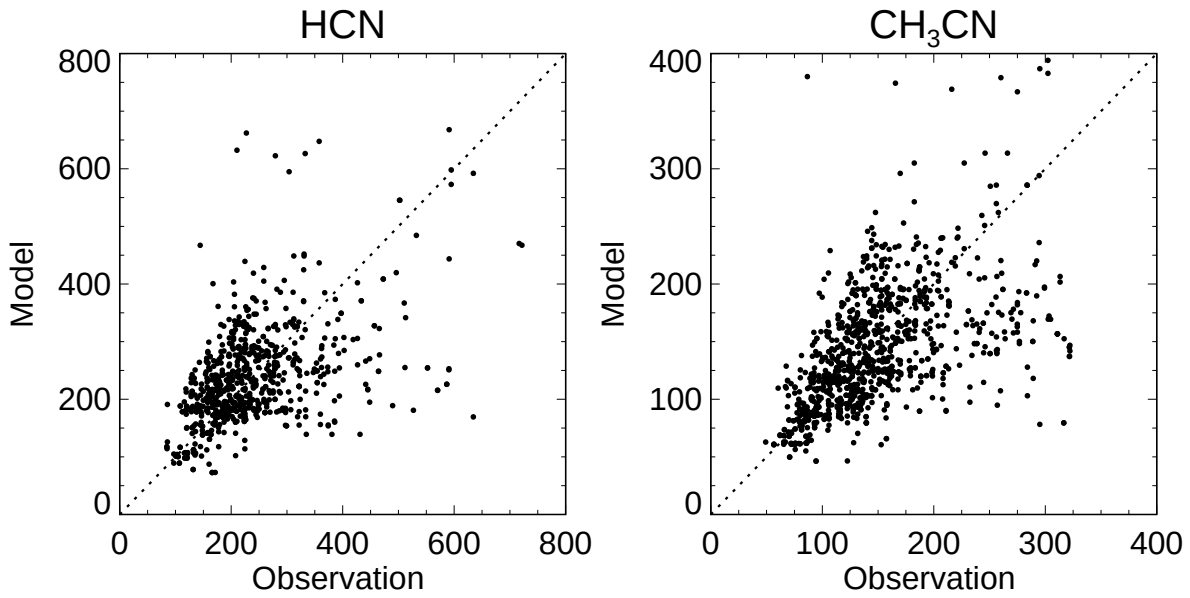

Figure 7. Scatterplots of simulated versus observed mixing ratios of HCN and CH_3CN for the ensemble of TRACE-P data. The 1:1 line is also shown.

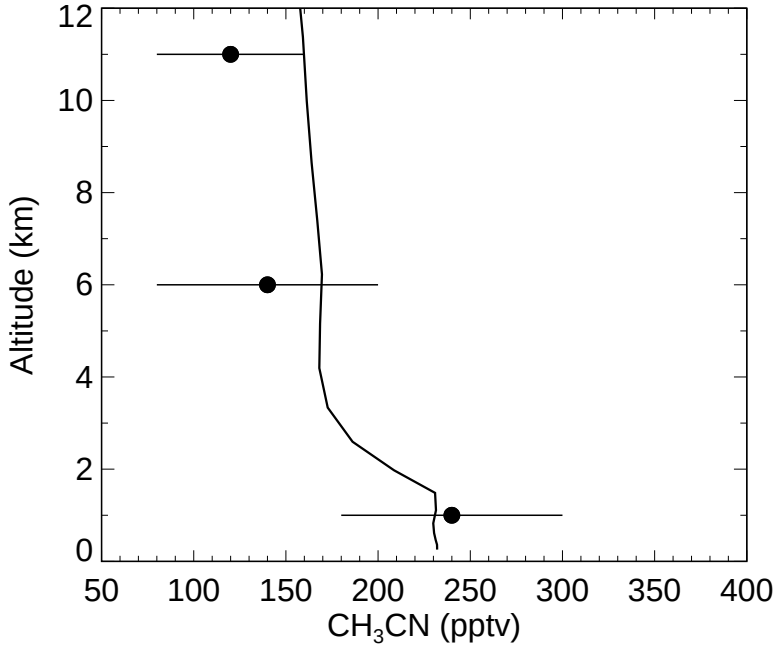

Figure 8. Vertical distribution of CH_3CN concentrations over the northern Indian ocean in March 2001. Median aircraft observations from the INDOEX campaign [*de Laat et al.*, 2001] are shown as symbols with standard deviations. Monthly mean model results for the corresponding month and region (0-10°N, 65-80°E) are shown as the solid line.

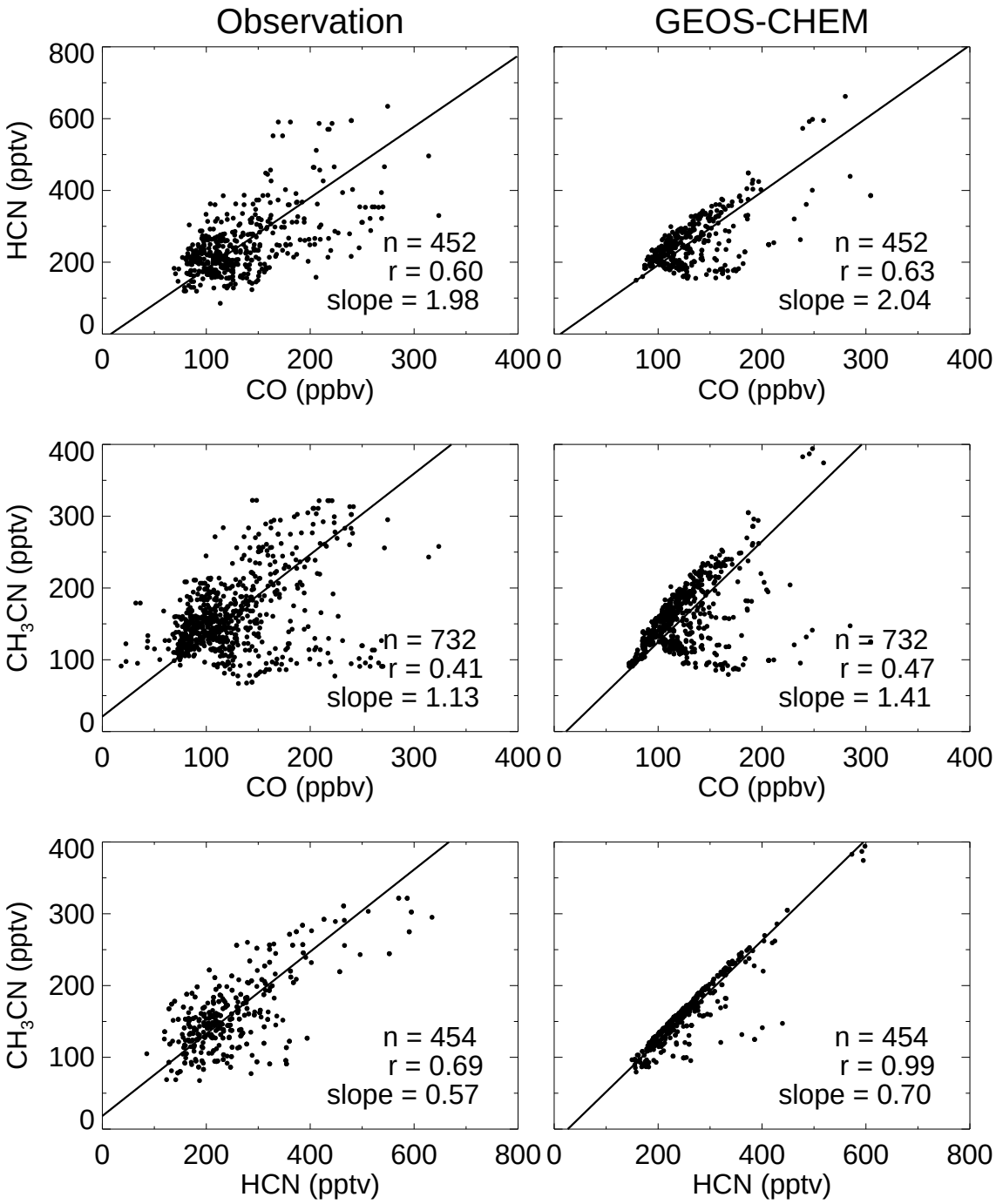

Figure 9a. Observed and simulated HCN-CH_3CN-CO correlations in the free troposphere (above 2 km) during TRACE-P. Regression lines and correlation coefficients are shown.

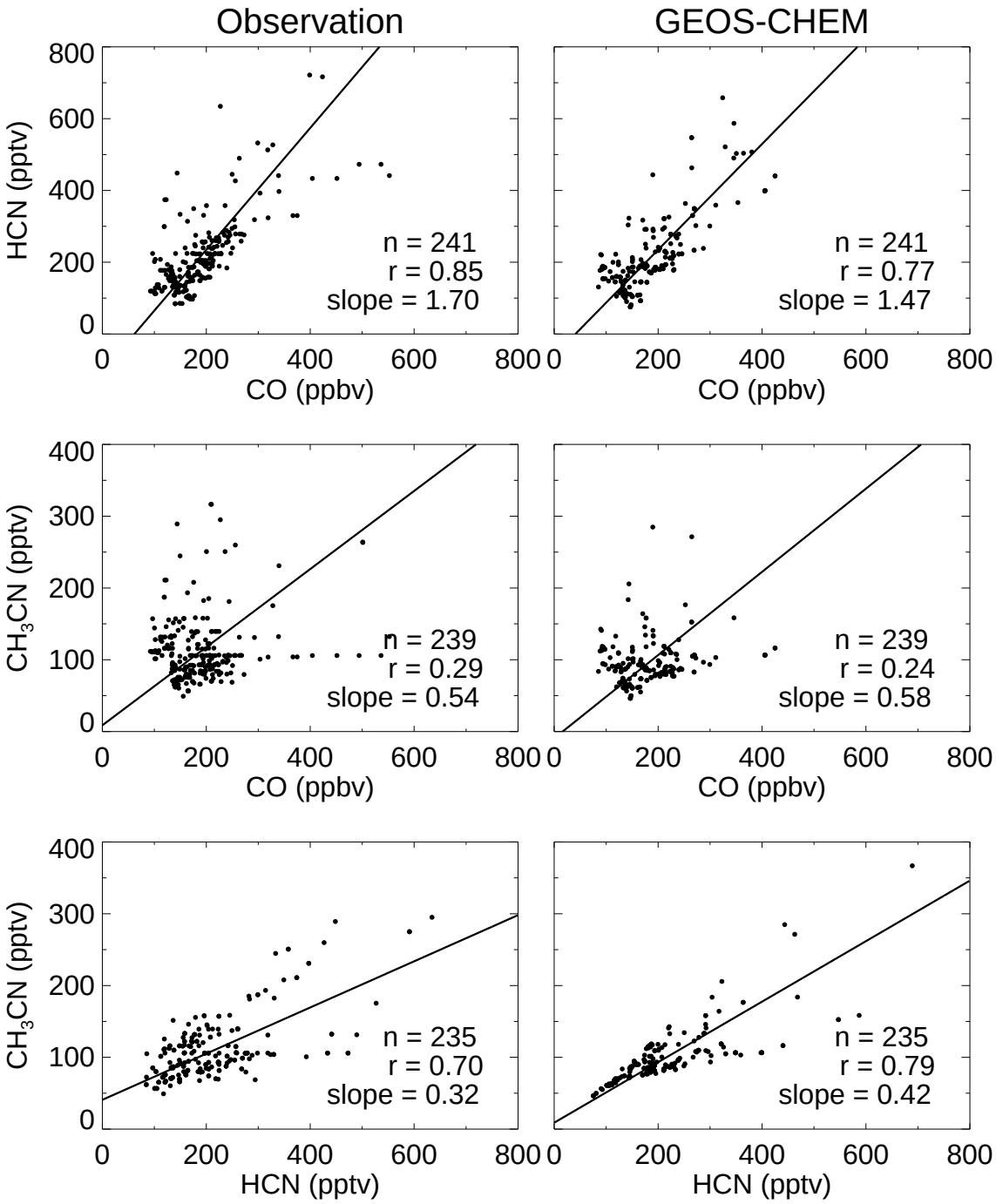

Figure 9b. Same as Figure 9a but the boundary layer (below 2 km).

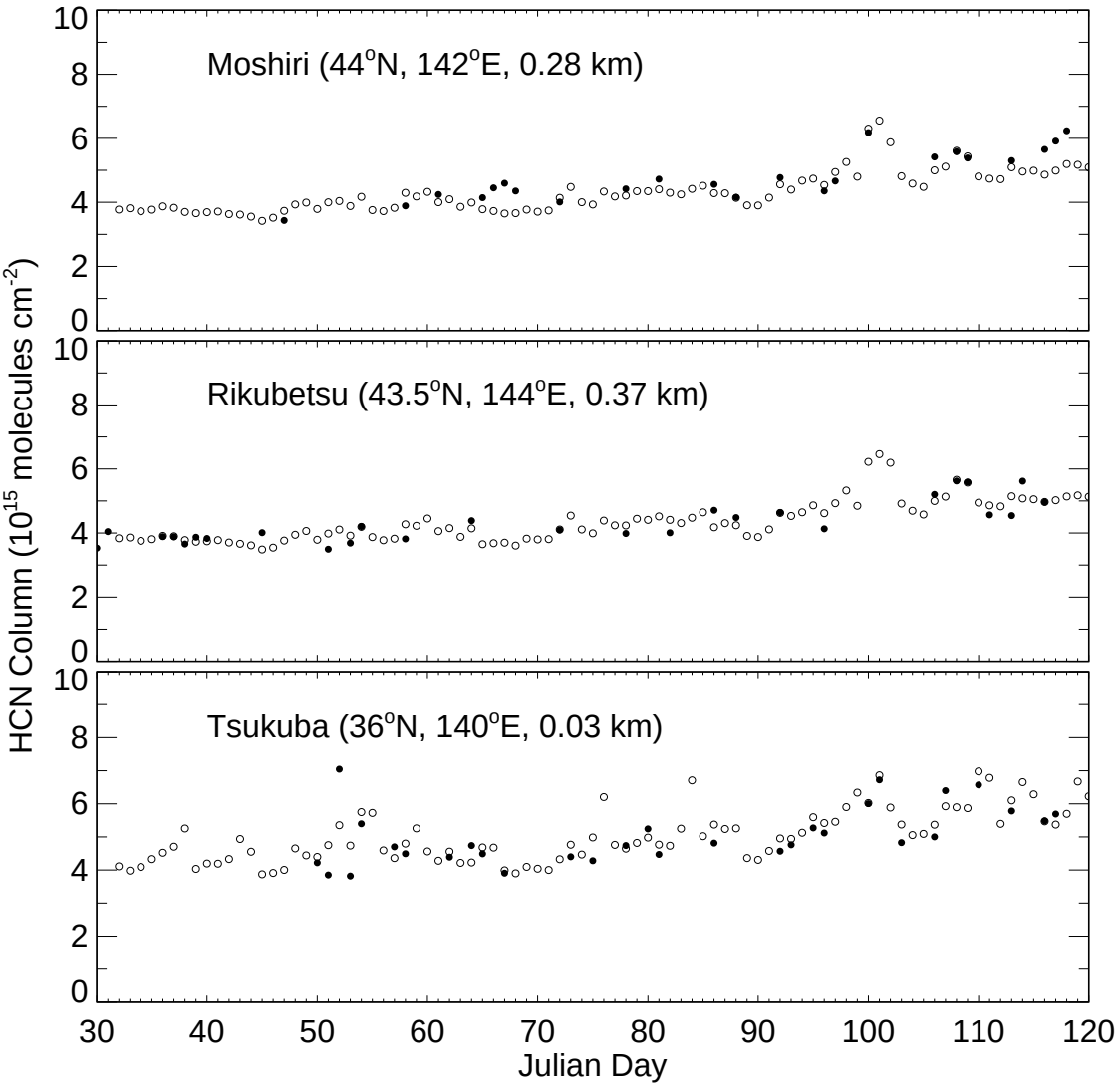

Figure 10. Time series of observed (solid circles) and simulated (open circles) 24-hour average HCN columns (molecules cm^{-2}) at the three Japanese stations of Moshiri (44°N, 142°E, 0.28 km altitude), Rikubetsu (43.5°N, 144°E, 0.37 km altitude), and Tsukuba (36°N, 140°E, 0.03 km altitude) during TRACE-P (February-April 2001).

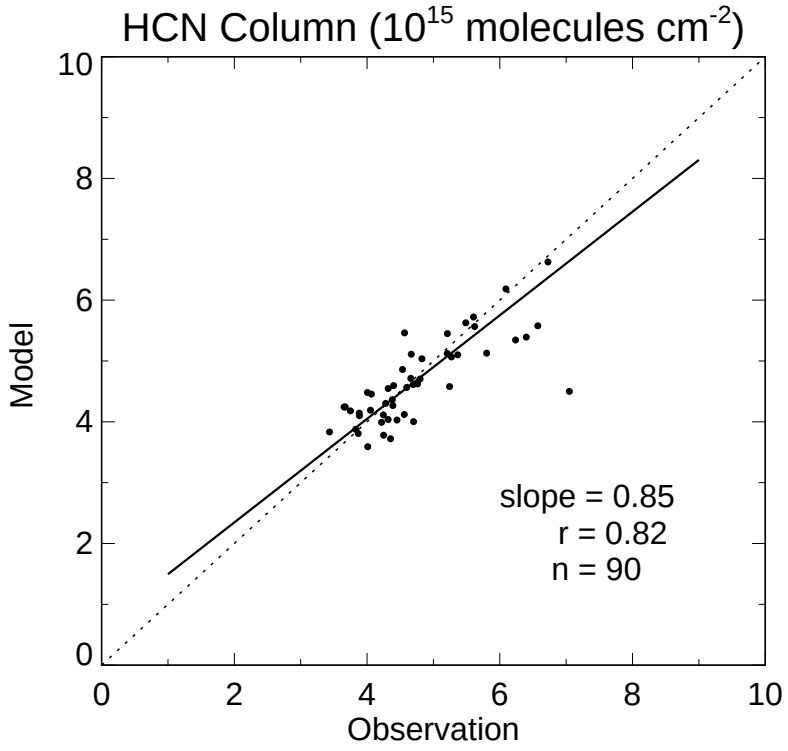

Figure 11. Scatter plot of observed and simulated daily HCN columns (molecules cm^{-2}) at Moshiri, Rikubetsu, and Tsukuba in TRACE-P. Values are averages over the three sites. The regression line is calculated without the outlier.

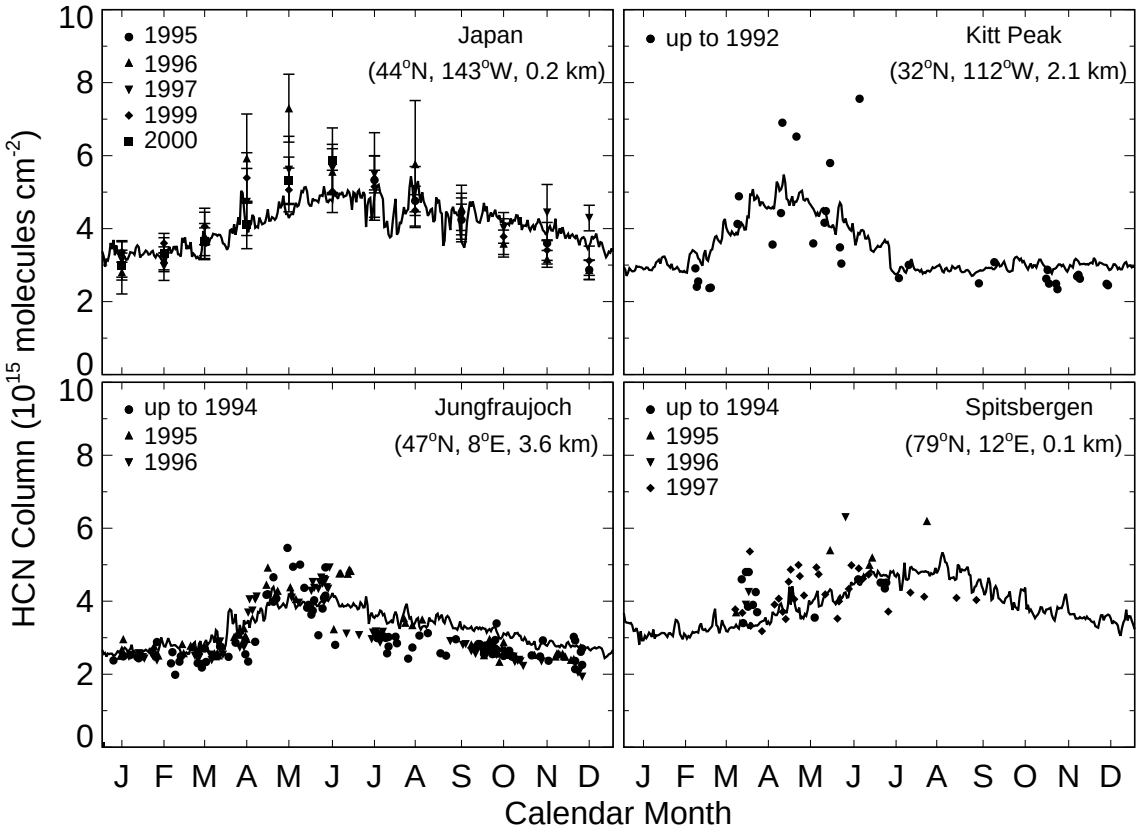

Figure 12. Monthly mean HCN total columns (molecules cm^{-2}) retrieved from spectroscopic measurements at Moshiri and Rikubetsu in Japan [*Zhao et al.*, 2000, 2002], Kitt Peak in Arizona [*Mahieu et al.*, 1995], Jungfraujoch in the Swiss Alps [*Mahieu et al.*, 1995, 1997], and Ny Ålesund in Spitsbergen [*Li et al.*, 2000]. Data for the two Japanese sites are monthly means and vertical bars indicate standard deviations. The solid lines represent simulated daily average HCN total columns for 2000.

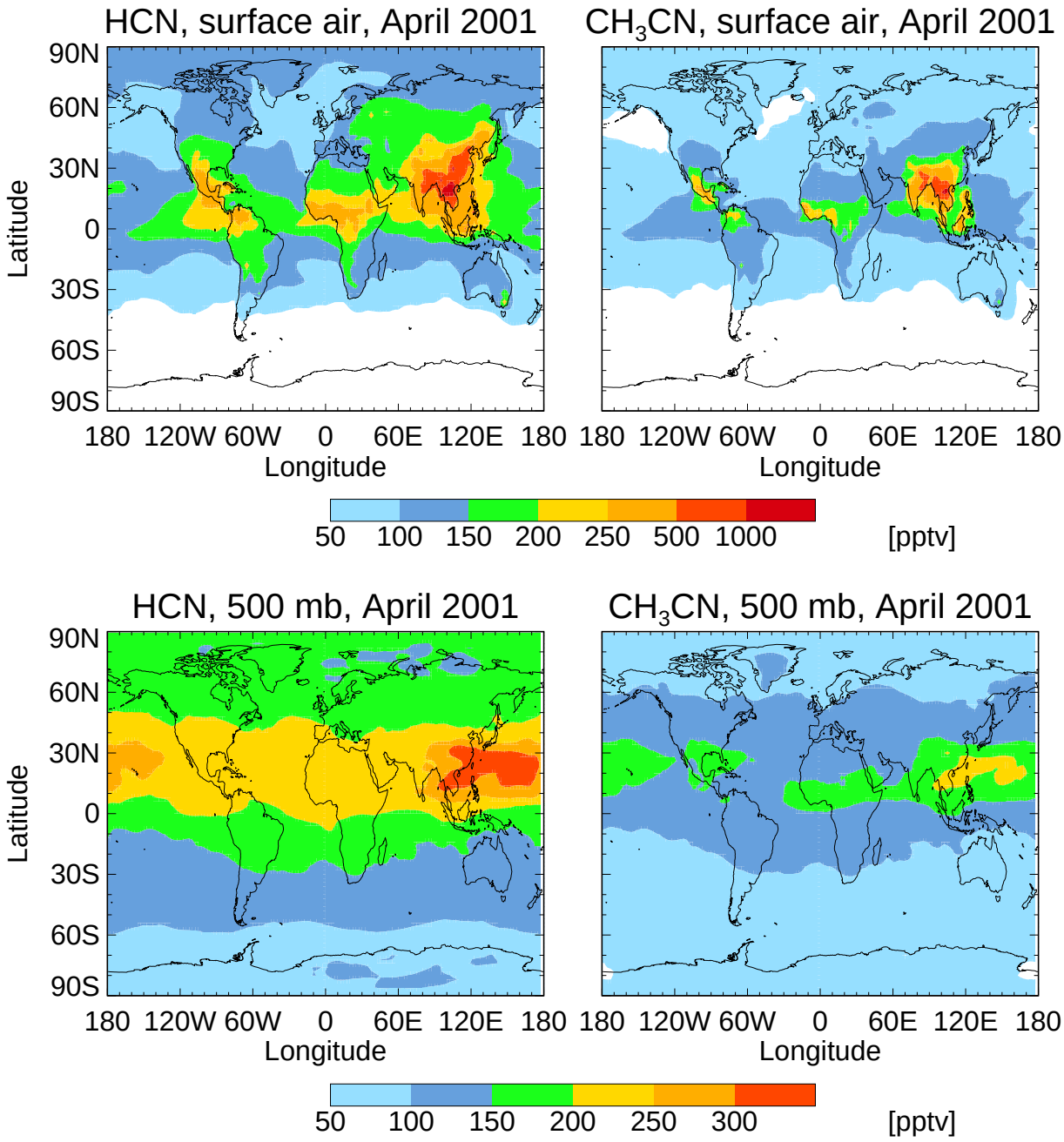

Figure 13. Simulated monthly mean concentrations of HCN and CH_3CN in surface air and at 500 hPa for April 2001.